Published in International Journal of Rock Mechanics & Mining Sciences, 71, 117-130, 2014
which should be used for any reference to this work

Distinct element method simulation of an analogue for a highly interlocked, non-persistently jointed rockmass

Navid Bahrani [a,b,*], Peter K. Kaiser [b,c], Benoît Valley [d]

[a] Geomechanics Research Centre, MIRARCO – Mining Innovation, Sudbury, Ontario, Canada
[b] Bharti School of Engineering, Laurentian University, Sudbury, Ontario, Canada
[c] Rio Tinto Centre for Underground Mine Construction, CEMI, Sudbury, Ontario, Canada
[d] Geological Institute, ETH Zürich, Zürich, Switzerland

Keywords:
Grain-based model
Calibration
Non-persistently jointed rockmass
Interlocking
Confinement

A B S T R A C T

A grain-based distinct element model is used to reproduce the laboratory response of both intact and granulated Wombeyan marble. The term "granulated" refers to a heat treated marble where the cohesion of grain boundaries has been destroyed. The unconfined compressive strength of granulated marble is less than 50% of that of intact marble, while the strength of the granulated marble increases to about 80% of that of the intact marble at higher confining stresses. An iterative calibration approach is developed to match the unconfined and confined strengths of the models to those of intact and granulated marble. The simulation test results of the models of intact and granulated marble including the transition in the failure mode, stress–strain response, and the evolution of inter- and intra-grain micro-cracks with increasing confinement are discussed. The observed rapid strengthening effect, in terms of increasing confinement, is interpreted to be due to the high degree of grain assembly geometric interlock, which arises from the tight fit geometric shape of the grains as well as the roughness of the grain boundaries. It is suggested that the granulated marble can be considered to be an analogue for a highly interlocked, non-persistently jointed rockmass. It is shown that when the generalized Hoek–Brown failure criterion and the Geological Strength Index (GSI) are used to match the strength of the granulated marble at zero confinement, the confined strength of the granulated marble is underestimated by as much as a factor of two. Therefore, the confined strength of a highly interlocked, non-persistently jointed rockmass, with strong, brittle rock blocks, could be significantly higher than that predicted by commonly adopted empirical approaches. This has practical implications for the design of highly confined pillars and abutments, which is discussed in this paper.

1. Introduction

The Geological Strength Index (GSI) rockmass characterization system [1,2] and the Hoek–Brown failure criterion [3–5] have been introduced to estimate the strength of isotropic, persistently jointed rockmasses. This approach was developed based on experience at shallow depths or low stress relative to the rockmass strength, rock strength back-analyses of near excavation wall behavior, and mostly for case examples with GSI-values up to 75 (i.e., in well to poorly interlocked rockmasses with fully persistent discontinuity networks). The use of this approach for the estimation of rockmass strength, when non-persistently jointed and highly interlocked (i.e., GSI-values greater than 75), and at great depth when highly confined (e.g., as encountered in squat pillar cores and abutments) is currently outside the experience base and therefore not supported by field evidence.

It is known that the failure process of intact rocks changes with increasing confinement as investigated in the laboratory experiments by Paterson [6] and many others. At great depth, the in situ stresses reach or even exceed the maximum confinement levels typically applied to rock cores in the laboratory, from which rockmass strength is estimated. To the knowledge of authors, no published strength test data exists for jointed rockmasses at high confining stress levels. Therefore, confined rockmass strength can only be obtained from back-analyses of wide, marginally stable pillars and abutments or, by extrapolation from physical models of jointed rockmasses or laboratory tests on damaged and defected rocks. Laboratory testing on samples at rockmass scales is expensive and time consuming, and most facilities cannot test hard

* Corresponding author at: MIRARCO – Mining Innovation, Laurentian University, 935 Ramsey, Lake Road, Sudbury, ON, Canada P3E 2C6. Tel.: +1 705 675 1151x5115.
E-mail address: nbahrani@mirarco.org (N. Bahrani).

rocks at high confinement levels. Laboratory data is extremely limited and cannot typically be generalized for rockmasses with discontinuity networks of different surface conditions and block interlocking levels.

Recently, numerical methods have been extensively used as an alternative approach to simulate jointed rockmasses at different scales. The discontinuous nature of rockmasses can be simulated by explicitly assigning discontinuities to the models using Discrete Fracture Network (DFN) [7,8]. A DFN allows for the consideration of the rockmass discontinuity fabric including its geometry (length, orientation, and persistence) at desired scales. However, the rough nature of the discontinuities, the related block interlocking and dilatant characteristics are usually ignored or suppressed in these simulations. In addition, numerical models are typically calibrated on rockmass behavior at low confinement (e.g., tunnel wall instability or narrow pillar failures) and this may lead to incorrect estimation of the confined strength of jointed rockmass.

A promising approach to assess the strength of jointed rockmasses is to numerically simulate laboratory tests on materials that can be considered to be an analogue of such rockmasses. Once the numerical model is calibrated, it can be used to simulate rockmasses with different block interlocking levels and joint surface conditions. In this study, a numerical model based on Distinct Element Method (DEM) is used to simulate the laboratory response of intact and heat treated marble. The heat treated marble is considered to be an analogue for a highly interlocked and non-persistently jointed rockmass; specifically a rockmass with relatively short joints that terminate on other joints. The challenge was to calibrate the numerical model to laboratory properties of both intact and heat treated marble in such a manner that the simulation results are independent of the applied stress path (i.e., model results match direct tensile, unconfined and confined compressive strengths of both intact and heat treated marble). The calibration procedure to choose the micro-properties of the models is first summarized. The transition in the failure modes, stress–strain response as well as the evolution of inter- and intra-grain micro-cracks with increasing confinement predicted by the calibrated models are also described. Finally, the implications of the laboratory test and modeling results for the estimation of the rockmass strength over the entire confinement range as well as for pillar design are discussed.

2. Strength of non-persistently jointed rockmass

2.1. Rockmass analogy

The generalized form of the Hoek–Brown (HB) failure criterion [5], which is widely used to estimate the strength of jointed rockmass is described by

$$\sigma_1 = \sigma_3 + \sigma_{ci}[m_b(\sigma_3/\sigma_{ci}) + s]^a \quad (1)$$

where σ_1 and σ_3 are respectively the maximum and minimum effective principal stresses at failure, σ_{ci} is the compressive strength of the intact rock pieces at zero confinement, and m_b, s and a are empirical constants. The value of m_b describes the slope of the failure envelope, s corresponds to the cohesive strength component, and a defines the curvature of the failure envelope. These parameters can be derived from the Geological Strength Index (GSI) introduced by Hoek [1] and Hoek et al. [2] to characterize the rockmass as a function of rock block interlocking level and joint surface conditions. The HB parameters are described by the following semi-empirical equations [9]:

$$m_b = m_i \exp[(\mathrm{GSI} - 100)/(C_m - 14D)]; C_m = 28 \quad (2)$$

$$s = \exp((\mathrm{GSI} - 100)/(C_s - 3D)); C_s = 9 \quad (3)$$

$$a = (1/2) + (1/6)[\exp(-\mathrm{GSI}/15) - \exp(-20/3)] \quad (4)$$

In these equations, D is a factor that depends upon the degree of disturbance to which the rockmass has been subjected by blast damage and stress relaxation.

Bahrani and Kaiser [10] analyzed the laboratory test data of intact and jointed Panguna Andesite [3,4], which was used at the early development stages of the HB failure criterion. They also reviewed the case histories, where HB failure criterion and the GSI system were used to estimate rockmass strength, and suggested that, since the available data and the case histories were used to estimate rockmass strength at low confinement, the HB failure criterion with the above quoted equations may not be applicable for estimation of confined rockmass strength. Furthermore, Bahrani and Kaiser [10] gathered previously published laboratory test results on intact and fractured rock samples and investigated the applicability of the HB failure criterion and the GSI system for strength estimation of non-persistently jointed rockmass. The laboratory tests reviewed by them were intact and heat treated Wombeyan marble [11–13], intact and granulated Carrara marble [12,13], and intact and artificially slotted fine and coarse grain marble [14]. The laboratory test results showed that the strength of a fractured sample, an analogue for a non-persistently jointed rockmass, increases more rapidly with confinement than that predicted by empirical methods, and approaches that of intact rock.

Bahrani and Kaiser [10] found that when the GSI-based HB failure criterion is used to match the strength reduction of fractured rock from intact rock at zero confinement, the strength of fractured rock estimated by Eqs. (1)–(4) at high confinement is underestimated by a factor of as much as two. They found that a much greater m_b-value than that estimated from Eq. (2), and a lower a-value than that estimated from Eq. (4) would be needed to reflect the high curvature at low confinement.

2.2. Laboratory properties of intact and granulated Wombeyan marble

The laboratory behavior of coarse-grained Wombeyan marble has been studied by Paterson [6], Rosengren and Jaeger [11], Gerogiannopoulos [12], and Gerogiannopoulos and Brown [13]. The confinement in the triaxial tests on intact marble performed by Paterson [6] ranged from 0 to 100 MPa. He observed a transition in the failure mode from axial fracturing in the unconfined compressive test to a well-defined single shear plane at low confinement (i.e., 3.5 MPa), to conjugate shear banding at higher confinement (i.e., 34.5 MPa), and to ductile behavior at extremely high confinement levels (i.e., 100MPa).

Rosengren and Jaeger [11] and Gerogiannopoulos [12] performed laboratory tests on intact and heat treated samples of marble up to a confinement of 34.5 MPa. Microscopic examination of thin sections of heat treated marble showed that due to the anisotropy of thermal expansion of calcite, the grains separated along their boundaries when the Wombeyan marble was heated to around 600 °C. For the heat treated marble, nearly zero tensile strength was measured in direct tension test with failure occurring by fracturing along the grain boundaries. The heat treated marble is referred to as “granulated” marble and it is suggested by Rosengren and Jaeger [11] that it can serve as an analogue for a jointed rockmass.

The laboratory test data for intact and granulated marble by Rosengren and Jaeger [11] and Gerogiannopoulos [12] are shown in Fig. 1(a) and (b), respectively. As can be seen, the unconfined compressive strength (UCS) of the granulated marble is reduced to

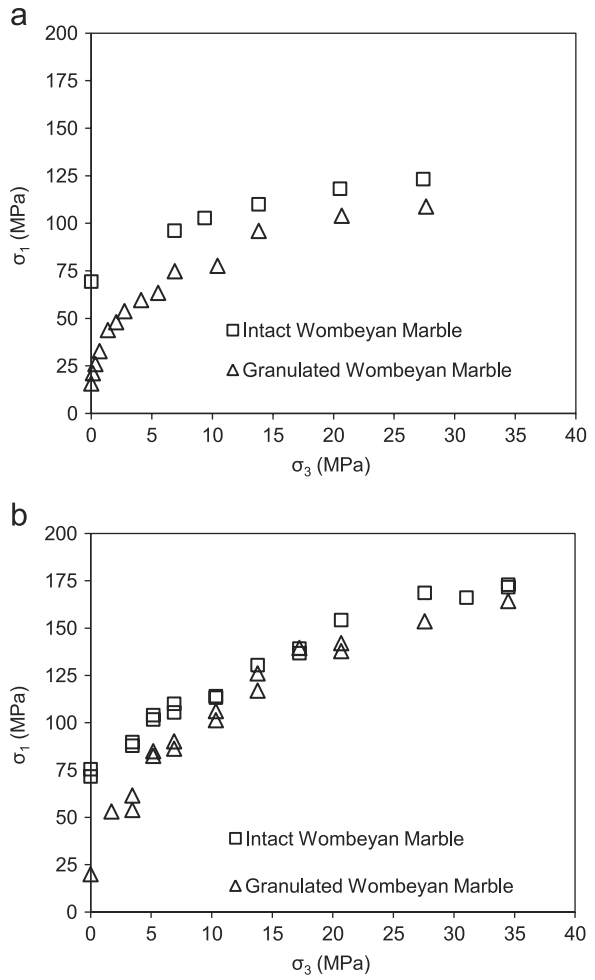

Fig. 1. Triaxial test results of intact and granulated coarse-grained Wombeyan marble reported by (a) [11] and (b) [12].

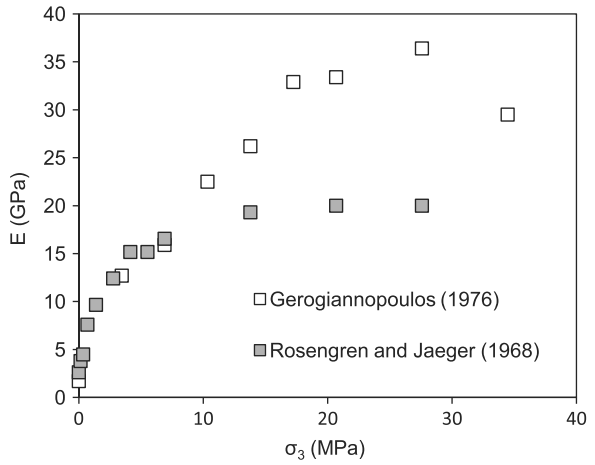

Fig. 2. Dependency of Young's modulus of granulated marble on confinement.

less than half of its intact UCS. However, with increasing confinement the strength of the granulated marble increases more rapidly than that for the intact marble. For confining pressures greater than about 5–10 MPa the strength of the granulated marble approaches about 80% of that of the intact marble.

Fig. 2 shows that Young's modulus of the granulated marble increases rapidly with increasing confinement and reaches a plateau of around 20 GPa and 30 GPa at confining pressures greater than 10 MPa and 15 MPa in the laboratory tests performed by Rosengren and Jaeger [11] and Gerogiannopoulos [12], respectively. Martin and Stimpson [15] observed a similar behavior on intact and damaged samples of Lac du Bonnet (LdB) Granite. They found that Young's modulus of samples damaged during coring from high stress ground is strongly confinement-dependent; it increases from about 35 GPa under unconfined condition to about 63 GPa at 10 MPa confining pressure and remains relatively constant beyond this confinement, and never reaches that of intact samples with an average value of 68 GPa over the entire range of confinement.

In this study, a grain-based model, where a rock is simulated with its deformable and breakable grains is used to simulate the laboratory behavior of the intact and granulated Wombeyan marble investigated in [12].

3. Modeling brittle rock in particle flow code (PFC)

The DEM developed by Cundall [16] is a numerical method that is capable of simulating irregular shaped particles for the analysis of rock mechanics problems. It was first applied to soils with circular particles by Cundall and Strack [17]. One of the applications of DEM is the simulation of intact rocks and rockmasses by considering the rock as an assemblage of circular or spherical particles, cemented at their contact points. This method, which is called the Bonded Particle Model (BPM), has been implemented in two- and three-dimensional codes PFC2D and PFC3D [18,19]. The PFC has been extensively used over the past two decades to study a wide range of rock mechanics phenomena as reviewed by Potyondy and Cundall [20] and Potyondy [21]. They illustrate that such a modeling approach can capture and simulate many aspects of the mechanical behavior and failure processes of brittle rocks from the laboratory to rockmass scale.

3.1. Calibration of PFC model to laboratory properties of intact rock

Calibration of a BPM is usually carried out by manually adjusting the micro-properties of the particles and the bonds until the macroscopic properties of the BPM match those of rock samples. Typically, the BPM is calibrated to the rock's UCS. Diederichs [22] and Potyondy and Cundall [20] showed that when a BPM is calibrated to the UCS, its tensile strength is significantly overestimated, the confined strength of the BPM is underestimated (i.e., low friction angle) and the resulting failure envelope is linear. The 3D DEM code developed by Wang and Tonon [23] showed improvement in the calibration results in terms of friction angle. However, the tensile strength of the BPM was found to be high compared to that of experimental results. Other criteria such as stress–strain curves (e.g., axial, lateral and volumetric strains), failure modes (e.g., progression of strain localization) and post-peak response have also been suggested for calibration of the BPMs [24].

Yoon [25], Wang and Tonon [23,26] developed methodologies for calibrating 2D and 3D BPMs based on optimization process, and by obtaining relationships between micro-properties and macro-properties through parameter sensitivity analysis. Yoon [25] showed the applicability of his method for calibrating the BPM to laboratory properties of rock materials with UCS ranging from 40 MPa to 170 MPa, Young's modulus ranging from 20 GPa to 50 GPa, and Poisson's ratio ranging from 0.19 to 0.25. The calibration process suggested by Wang and Tonon [26] showed reasonable agreement between simulated and experimental results in terms of deformability and unconfined and confined strengths.

Cho et al. [27] questioned the calibration process which is based on matching the UCS and suggested that such a calibrated

model would only be adequate for simulating materials under unconfined conditions and only for tests in compression. In an effort to solve the limitations of the BPM mentioned above, they proposed an approach where a number of particles are glued together to generate a clump with a complex shape. The clumped particle model (ClmPM) consists of a number of bonded clumps and each clump represents a rock grain, which moves as a single rigid object. Cho et al. [27] found good agreement between the tensile strength, the UCS, and the confined strength of the ClmPM and those of LdB granite. The ClmPM has also been used by Yoon et al. [28,29] to reproduce not only the UCS, Young's modulus and Poisson's ratio, but also crack initiation and crack damage thresholds of Aue granite. In their modeling, matching the Brazilian tensile strength was not successful [29]. However, Yoon et al. [28] was able to match the Brazilian tensile strength of Aue granite by unbonding certain amount of bonds in the ClmPM.

Since the clumps are unbreakable and rigid, the calibration of the ClmPM requires adjustment of the micro-properties representing those of rock grain boundaries (i.e., strength and stiffness), but not the grains. However, due to the number of micro-parameters the solution is in general not unique and different combinations of micro-properties can result in the same macro-properties. As a means to reduce the number of possible solutions Bahrani et al. [30] proposed an approach, whereby the ClmPM macro-properties are calibrated to laboratory properties of intact and damaged rock samples (i.e., LdB granite) through an iterative adjustment of the micro-properties of the ClmPM.

A major practical limitation of the ClmPM is that the grains are rigid and unbreakable. Laboratory tests have shown that this is not a realistic assumption as grain crushing occurs in compression tests [31,32], especially at high confinement [33]. Similarly, when a rockmass fails, rock blocks, and not just block boundaries, fail. To resolve this issue, Potyondy [34] developed a methodology in PFC2D, where a rock is simulated by deformable and breakable polygonal grains. The results of the calibration of the grain-based model (GBM) to laboratory test results of ÄspÖ Diorite, Wombeyan marble, LdB granite, Lodève sandstone have been reported by Potyondy [34], Bahrani et al. [35], Bahrani et al. [36], and Bewick et al. [37,38], respectively. For the GBM with breakable grains, the micro-properties of both grains and grain boundaries must be defined. Therefore, the number of micro-properties in the GBM with breakable grains is about two times that of the ClmPM. This drastically increases the non-uniqueness of the solution, when the GBM with breakable grains is used.

In the following, a methodology for the calibration of the GBM with breakable grains is presented to minimize the number of possible solutions. A systematic and iterative calibration procedure, similar to that adopted by Bahrani et al. [30,35], is used to match the macroscopic properties of the GBM to those of intact and granulated Wombeyan marble.

3.2. Grain-based model in PFC2D

The grain-based model in PFC2D [34] is a synthetic material that simulates a rock with an assembly of deformable, breakable, polygonal grains. The grain structure generation procedure described by Potyondy [34] is summarized as follows. The generation of the grain structure first requires a bonded particle (ball) model with no walls. The balls must have at least two contacts. Each contact joins two balls. An example of a PFC2D model is shown in Fig. 3(a), where each contact is depicted as a line joining the centers of its two contacting particles. A void is defined as a closed chain of balls and contacts. Each contact is adjacent to two voids. There is one external void that encircles the entire system and many internal voids. Each internal particle (defined as a particle that is not adjacent to the external void) corresponds with a grain whose edges join the internal-void centroids (Fig. 3(b)). Internal balls with less than three contacts are removed before generating the grains. The grain structure is a polygonal mesh that completely fills space (Fig. 3(c)). The GBM is then generated by overlaying the grain structure on a conventional BPM, (ball model, called the base material) with a number of smaller balls to fill the grains. The balls inside the grains are bonded using parallel bonds and this produces deformable and breakable grains. The grain structure is replaced by smooth-joint contacts. An illustration of a grain assembly with parallel bonds and smooth-joint contacts in a GBM is shown in Fig. 4(a) and (b).

In PFC2D, a parallel bond can be envisioned as a set of elastic springs, uniformly distributed over a rectangular cross section lying on the contact plane and centered at the contact point between two particles (Fig. 5(a)). The smooth-joint contact simulates the behavior of an interface regardless of the local particle contact orientation along the interface (Fig. 5(b)). The use of smooth-joint contacts to simulate the behavior of joints in a rockmass has been investigated by Hadjigeorgiou et al. [39], Esmaieli et al. [40], Mas Ivars et al. [8], and Chiu et al. [41].

Ball movements after breakage of parallel bonds and smooth-joint contacts are shown in Fig. 5(c) and (d). The strength of parallel bond and smooth-joint contact is defined by the tensile strength, cohesion and friction angle. When a parallel bond breaks (either in shear or tension), the residual strength is controlled by the friction coefficient of the balls in contact and the ball size, which generates a local dilation and causes the balls to move around each other (Fig. 5(c)). However, when a smooth-joint contact breaks (either in tension or shear), its residual strength is defined by the smooth-joint friction coefficient. The balls that are located on opposite sides of a smooth-joint plane can overlap to allow particle sliding along the joint plane (with no local geometric dilation as shown in Fig. 5(d) rather than forcing the balls to move around one another.

Once the smooth-joint is created, its stiffness properties are inherited from the contact and the two contacting balls, according to the following equations:

$$\overline{k}_n = (k_n/A) + \overline{k}^n \tag{5}$$

$$\overline{k}_s = (k_s/A) + \overline{k}^s \tag{6}$$

$$A = 2\overline{R}t, \quad t - 1.0 \tag{7}$$

$$\overline{R} = \overline{\lambda}\,\min(R^A, R^B) \tag{8}$$

where $\overline{k}_n$ and $\overline{k}_s$ are the smooth-joint contact normal stiffness and shear stiffness, respectively, k_n and k_s are the contact normal stiffness and shear stiffness, respectively, and $\overline{k}^n$ and $\overline{k}^s$ are the parallel bond normal stiffness and shear stiffness, respectively. A is the cross sectional area of the smooth-joint contact, t is the ball thickness, $\overline{R}$ is the smooth-joint contact radius (i.e., half length of smooth-joint contact) which is a multiple, $\overline{\lambda}$, of the two particle radii, R^A and R^B. The ball thickness and radius multiplier have a value of 1 by default. Note that the smooth-joint normal stiffness and shear stiffness are assigned as a factor of the stiffness inherited from the contact and the two contacting balls. This factor controls Young's modulus of the GBM and is called the stiffness factor in this paper.

4. Grain-based model of Wombeyan marble

4.1. Model geometry and grain structure

A 20 by 50 mm^2 GBM was used to simulate the laboratory behavior of intact and granulated marble. The size of the GBM

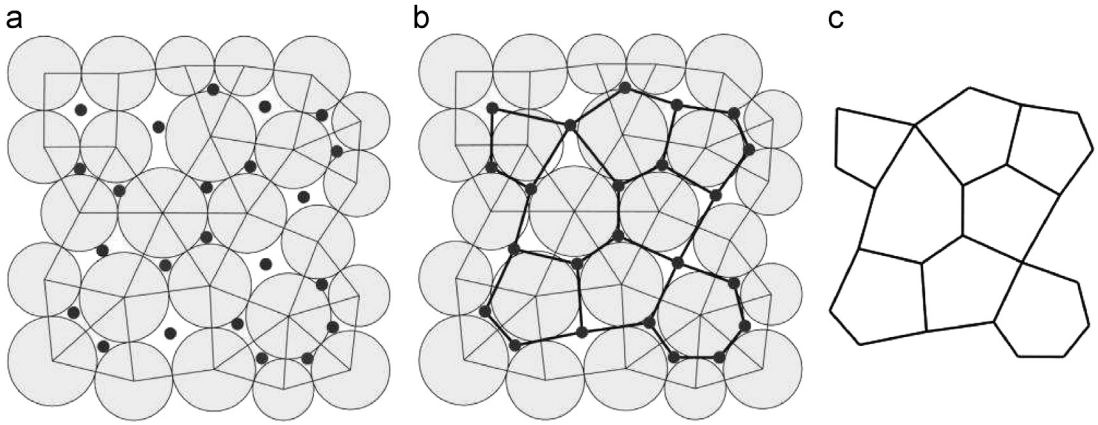

Fig. 3. Grain structure generation procedure: (a) initial ball packing showing balls and contacts with filled circles at internal-void centroids, (b) grain structure consisting of polygons, one for each internal ball, with nodes at internal-void centroids, and (c) final grain structure (after [34]).

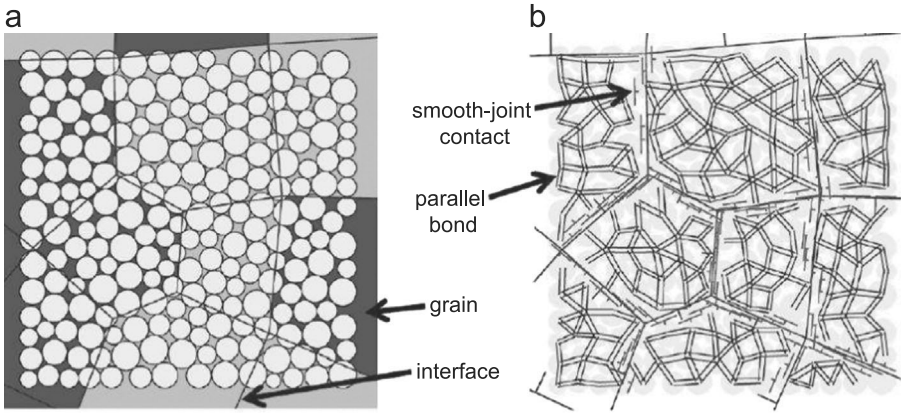

Fig. 4. (a) BPM overlaid on a grain structure. (b) PFC2D consisting of balls bonded together with parallel bonds inside the grains and smooth-joint contacts along the grain boundaries (after [34]).

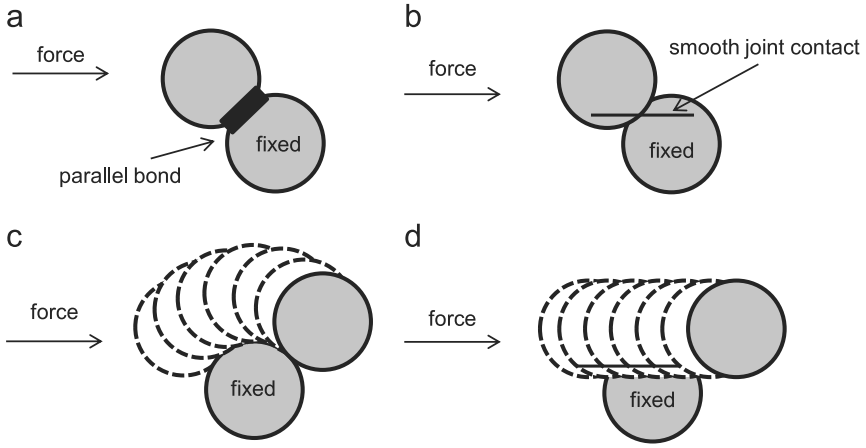

Fig. 5. Movements of balls after breakage of parallel bond and smooth-joint contact (after [42]).

chosen for simulation is smaller than the samples reported by Gerogiannopoulos [12]. This was required to reduce the calculation time while matching model grain size with actual rock grain size. According to Potyondy and Cundall [20], scale effects are not significant when modeling rocks in compressive loading conditions, provided the ball size is relatively small compared to the size of the model.

The average grain size of Wombeyan marble according to Gerogiannopoulos [12] and Rosengren and Jaeger [11] is between 1 and 2 mm. A simplified grain structure containing two different-sized equally and randomly distributed polygonal grains with average grain size of 1 and 2 mm was generated (Fig. 6(a)) according to the procedure described earlier. No attempt was made to match the grain size distribution of the GBM to that of Wombeyan marble. Moreover, to simplify the calibration process, only one grain type was considered in the GBM. Note that the ratio of the largest grain diameter to sample diameter used in the simulation is 0.1, which is in agreement with that suggested by the

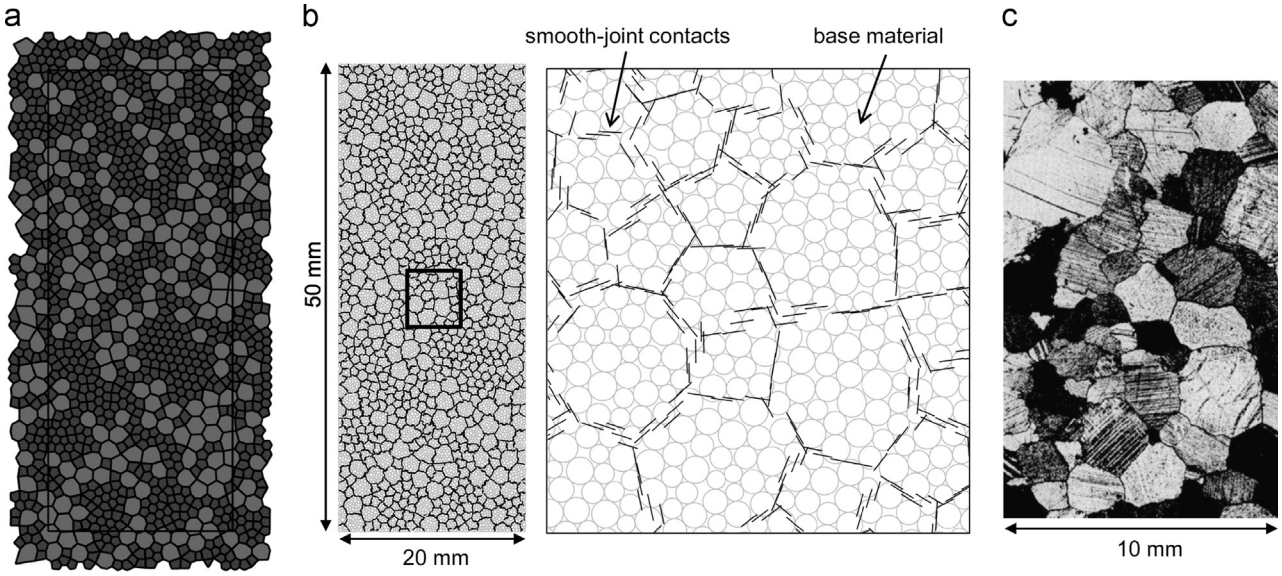

Fig. 6. (a) Modeled grain structure containing polygonal grains with average grain size of 1 mm (dark gray grains) and 2 mm (light gray grains), (b) grain-based model in which the grain structure is replaced by the smooth-joint contacts. The parallel bonds joining the balls inside the grains are not shown in this figure. (c) Micro-structure of Wombeyan marble (from [11]).

ISRM [43]. Furthermore, in the GBM generated (Fig. 6(b)), each grain is made of multiple balls with a maximum diameter of 0.4 mm. This ensures that the maximum ball size is smaller than the minimum grain size and that each grain is made of more than five balls. An example of the micro-structure of Wombeyan marble is shown in Fig. 6(c).

4.2. Calibration assumptions

The micro-properties of the GBM were obtained such that the macroscopic response of the model matches the observed macro-properties, i.e. the strength (uniaxial compressive, triaxial compressive, and tensile), and Young's modulus of both intact and granulated Wombeyan marble. In order to reduce the number of independent parameters, a number of assumptions on how some of the model micro-properties relate are made. In a previous attempt to simulate the laboratory behavior of intact and granulated Wombeyan marble reported by Gerogiannopoulos [12], Bahrani et al. [35] had to use different values of friction angle for smooth-joint contacts (grain boundaries) to achieve proper match of the macro-properties for the models of intact and the granulated marble. They used peak smooth-joint friction angles of 35° and 75° in the models of intact and granulated marble, respectively. This assumption is not realistic as heating the marble should not affect the frictional properties of the grain boundaries, but only their cohesional strength component. Moreover, an angle of 75° is unrealistically high for the grain boundaries, even if it is assumed that it represents an equivalent friction of $\phi + i$, where i is the dilation angle. In order to remediate to these limitations, the calibration procedure and underlying assumptions made by Bahrani et al. [35] are revised as follows:

Assumption 1. It is assumed that heating intact marble samples only affects the mechanical properties of the grain boundaries, but not the grains (i.e., by destroying the bonds between the grains). Therefore, the parallel bonds and balls (components of grain) were assigned the same micro-properties in the models of intact and granulated marble.

Assumption 2. The grain boundaries in the granulated marble have zero tensile strength and cohesion. Therefore, the normal (tensile) strength and cohesion of the smooth-joint contacts in the model of granulated marble were set to zero.

Assumption 3. Parallel bonds (bonds between the balls inside the grains) have the same normal (tensile) strength and shear (cohesion) strength in the models of intact and granulated marble.

Assumption 4. In the model of intact marble the smooth-joint contacts were assigned a zero friction angle (i.e., peak frictional strength component) and a non-zero friction coefficient (i.e., ultimate frictional strength component), as shown schematically in Fig. 7(a). This means that the strength of smooth-joint contacts is defined by cohesion, tensile strength and zero friction angle before contact failure, and by non-zero friction angle after contact failure. Therefore, at the grain scale, the transition to the ultimate strength is instantaneous and controlled by the smooth-joint friction coefficient when the smooth-joint breaks. In the model of granulated marble, the strength of smooth-joint is only defined by the friction coefficient (Fig. 7(b)).

Assumption 5. Similar to the smooth-joint contacts, the peak strength envelope of the parallel bonds is defined by non-zero tensile strength and cohesion and zero friction angle. The residual strength of balls previously bonded with parallel bonds is defined by the friction coefficient at ball–ball contacts and the ball geometry causing local dilation when the parallel bond breaks (see Fig. 5).

Assumption 6. Models of intact and granulated marble have the same ultimate frictional properties; the same friction coefficient for the smooth-joint contacts and the same friction coefficient for the balls. In the calibration process, the ultimate friction angle of the smooth-joint contacts (i.e., assigned as friction coefficient in the GBM) was considered to be the same as the equivalent friction angle of the granulated marble for the range of 0–7 MPa confinement with the value of about 50°.

Assumption 7. Parallel bonds and balls were assigned the same modulus in the models of intact and granulated marble.

Assumption 8. Parallel bonds, ball contacts and smooth-joint contacts were assigned the same normal to shear stiffness ratio in the models of intact and granulated marble.

The adopted behavior for smooth-joint contacts and parallel bonds indicates that at the sample scale, with increasing damage (increasing number of broken bonds), the cohesive strength component is gradually lost and the frictional strength component gradually mobilizes. This explicitly captures a fundamental characteristic of brittle rocks known as strain-dependent cohesion-weakening and frictional-strengthening [44,45].

The 'friction' angle of 50° for the grain boundaries in the model of granulated marble is not unrealistic if it is understood that the frictional strength consists of friction and dilation components, as explained by the bilinear shear strength envelope of Patton [46] for a rough discontinuity in direct shear. Such high equivalent friction angles have been previously observed in locked sands by Dusseault and Morgenstern [47,48], and LdB granite by Martin and Chandler [44]. In the GBM, the grain boundaries are modeled to be smooth surfaces using the smooth-joint contact logic, and therefore the roughness of the asperities along the grain boundaries is not explicitly simulated. The behavior of the granulated marble at low confinement had then to be replicated by increasing the 'friction' of the smooth-joints from the basic friction angle of 35° (obtained from the direct shear test by Gerrogianopoulos [12]) plus a dilation component of 15° to arrive at an 'equivalent friction' angle of 50° (i.e., smooth-joint friction coefficient of 1.2).

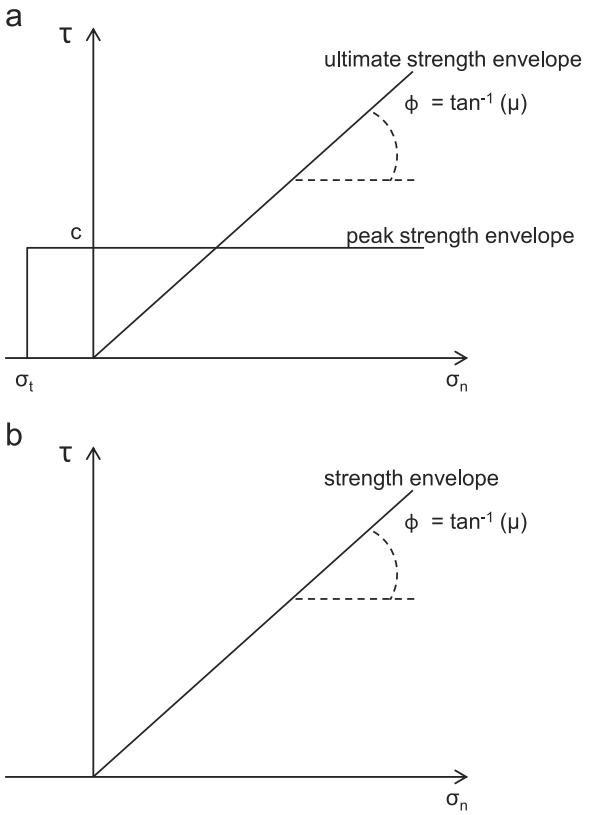

Fig. 7. Schematic strength envelopes for the smooth-joint contacts in: (a) model of intact marble and (b) model of granulated marble. Note that smooth-joint contacts are assigned the same friction coefficient in the models of intact and granulated marble.

4.3. Calibration procedure

Based on the assumptions mentioned above, the numbers of independent unknown micro-properties are 1 for the grain boundaries and 3 for the grains in the model of granulated marble, and 3 for the grain boundaries and 3 for the grains in the model of intact marble. The calibration process was started by adjusting the micro-properties of the model of granulated marble in a systematic manner as summarized in the flow chart shown in Fig. 8 and described in the following steps:

Step 1: Calibration on granulated marble tensile and unconfined compressive strengths, and Young's modulus: as a starting point, arbitrary micro-property values had to be chosen for the unknown parameters. The nearly zero tensile strength of the granulated marble was automatically achieved by assigning

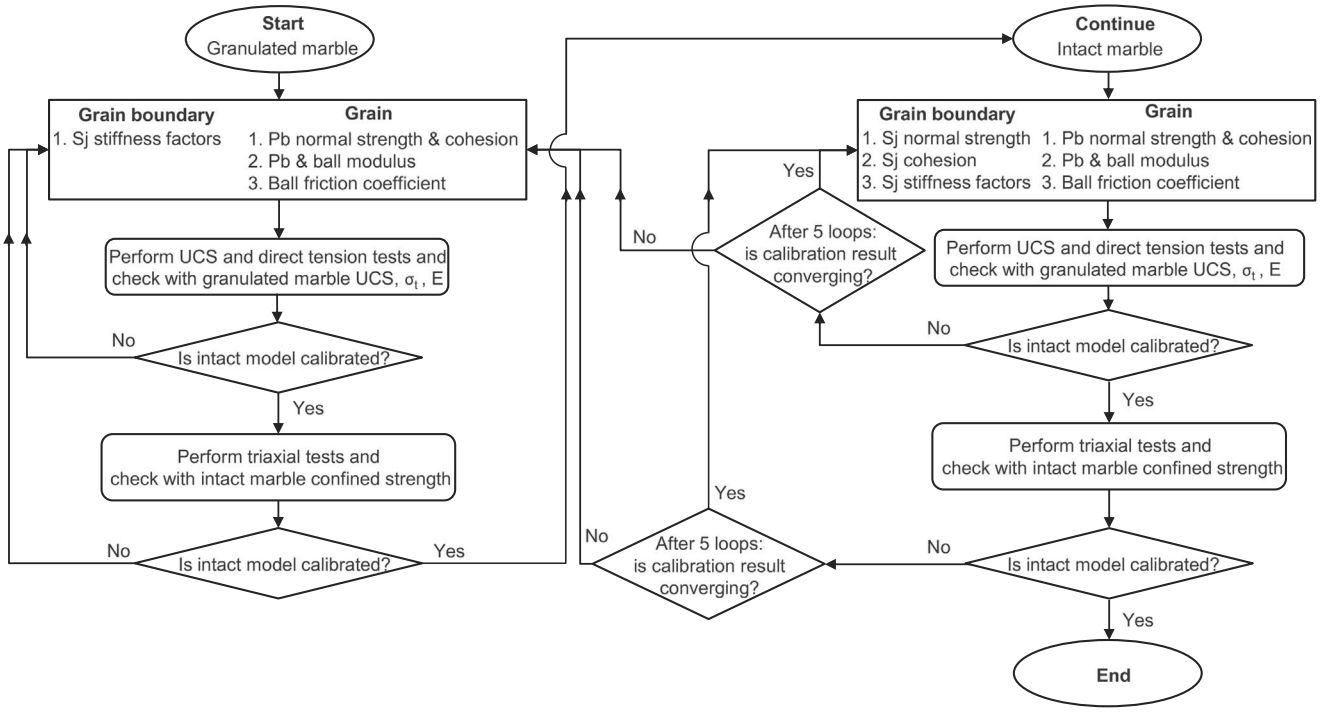

Fig. 8. Procedure for calibrating the grain-based model to laboratory properties of intact and granulated Wombeyan marble (Sj stands for smooth-joint and Pb stands for parallel bond).

zero normal (tensile) strength to the smooth-joint contacts. Since the values of the smooth-joint cohesion and friction coefficient have been defined in the assumptions for the model of granulated marble, the only micro-parameters that control the model of granulated marble uniaxial compressive strength were parallel bond normal (tensile) strength and cohesion (i.e., grain strength micro-properties). The Young's modulus of the granulated marble was obtained by adjusting the stiffness factor of smooth-joint contacts (see Section 3.2 for details on the stiffness factor). These parameters were manually adjusted until the tensile and unconfined compressive strengths, and Young's modulus of the model of granulated marble were matched with those of granulated marble (first internal loop for granulated marble in Fig. 8).

Step 2: Calibration on granulated marble confined strength: triaxial test simulations were then carried out with the parameters obtained from step one. The micro-properties of the grains including the parallel bond normal strength and cohesion, and ball friction coefficient affect the confined strength of the granulated model. Once changes in these parameters were made, step one was repeated to ensure GBM calibration with respect to strength and Young's modulus of granulated marble (second internal loop for granulated marble in Fig. 8).

Step 3: Calibration on intact marble tensile and uniaxial compressive strengths and unconfined modulus: the tensile strength of the model of intact marble was matched by adjusting the smooth-joint normal strength (Wombeyan marble tensile strength is 7 MPa according to Wei and Anand [49]). The UCS of the model of intact marble was found to be correlated to the smooth-joint cohesion, parallel bond normal strength and cohesion, and ball friction coefficient. The Young's modulus of the model of intact marble was also found to be correlated with the parallel bond and ball modulus as well as the smooth-joint stiffness factor (see Section 3.2 for details on the stiffness factor). At this stage, if a match with the properties of intact marble was not achieved (the micro-properties did not converge to target properties after five internal loops), calibration had to be redone from step 1 (first external loop in Fig. 8).

Step 4: Calibration on intact marble confined strength: the GBM which was previously calibrated to the intact marble unconfined compressive strength was tested for its confined strength. The confined strength of the model of intact marble is correlated to parallel bond normal strength, cohesion and ball friction coefficient. Similar to the previous step, if after five internal loops the model properties did not converge to the target properties, the calibration had to be redone from step 1 (second external loop in Fig. 8).

No information on the values of Poisson's ratio for the intact and granulated Wombeyan marble was found in the literature and therefore Poisson's ratio was not considered in the calibration process.

4.4. Calibration results

It should be noted that the confined modulus rather than unconfined modulus of the granulated marble was considered during the calibration process. This is due to the fact that the opening of the grain boundaries in the granulated marble caused by heating is not explicitly modeled, and therefore re-closure along the grain boundaries as a result of increasing confinement and applying axial load in unconfined and confined compression tests is not captured in the grain-based model of granulated marble. A smooth-joint stiffness factor of 0.2 was required to match the confined modulus of granulated marble. As a consequence and as shown in Fig. 9, the resulting modulus of the GBM corresponds with that of granulated marble at confining pressures greater than 17 MPa. It was found that only in this case can the unconfined and confined strengths of the models of intact and granulated marble be matched with those of Wombeyan marble test results as shown in Fig. 10. This figure also suggests that the direct tensile strength, the uniaxial compressive strength, reasonable friction angle as well as the non-linear failure envelope can be well captured by the GBM.

Tables 1 and 2 summarize the micro-properties of the grains and grain boundaries in the models of intact and granulated Wombeyan marble obtained through this calibration process. As shown in Table 1, the grains in both intact and granulated models were assigned the same micro-properties, based on the assumption that heating the intact marble did not affect the mechanical properties of the grains. Only changes in the smooth-joint properties, representing the grain boundaries, were required to simulate the transition from intact to granulated marble (Table 2). Also note that the smooth-joint contacts have the same frictional properties in the models of intact and granulated marble.

Once the calibration was completed, a conventional parallel bonded model (i.e., a PFC model with circular particles bonded together with parallel bonds) was generated with identical micro-properties as those of the grains in the calibrated GBM (i.e.,

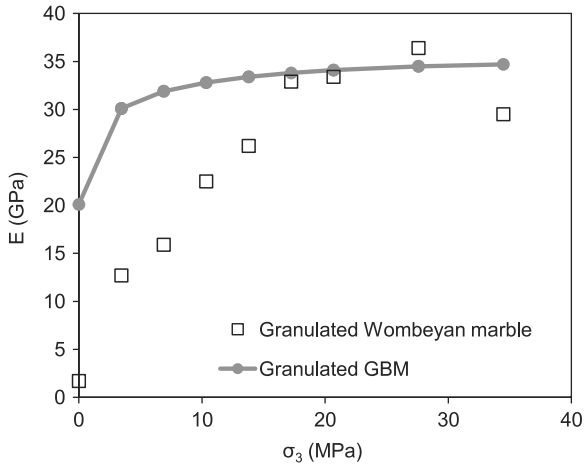

Fig. 9. Confined elastic modulus of granulated marble considered for calibration. In this case, the elastic modulus at low confinement is significantly overestimated by the GBM.

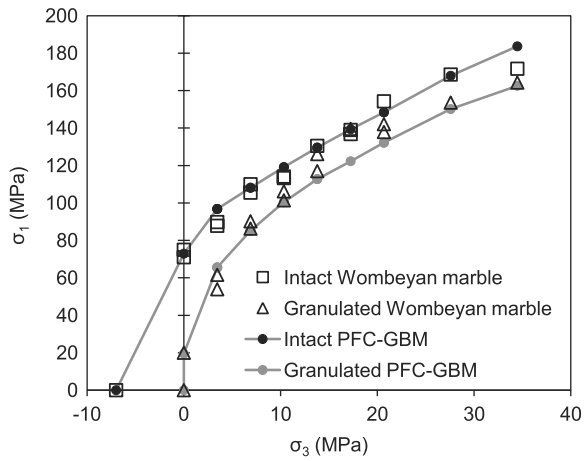

Fig. 10. Illustration of correspondence between unconfined and confined and tensile strengths of numerical simulation and laboratory test results of intact and granulated marble, when confined modulus of granulated marble is matched during calibration.

Table 1
Micro-properties of the grain in the models of intact and granulated marble.

Micro-properties	Intact and granulated GBM
Minimum particle (ball) radius	0.12 mm
Ratio of maximum to minimum ball radius	1.66
Contact normal to shear stiffness ratio	2.5
Parallel bond normal to shear stiffness ratio	2.5
Contact modulus	50 GPa
Parallel bond modulus	50 GPa
Ball friction coefficient	0.5
Parallel bond radius multiplier	1
Parallel bond normal (tensile) strength	110 MPa
Parallel bond cohesion	110 MPa
Parallel bond friction angle	0°

Table 2
Micro-properties of the grain boundary (smooth-joint contacts) in the models of intact and granulated marble.

Micro-properties	Intact GBM	Granulated GBM
Smooth-joint normal to shear stiffness ratio	2.5	2.5
Smooth-joint stiffness factor	0.8	0.2
Smooth-joint normal (tensile) strength	10 MPa	0 MPa
Smooth-joint cohesion	65 MPa	0 MPa
Smooth-joint friction angle	0°	0°
Smooth-joint friction coefficient	1.2	1.2

parallel bond normal strength and cohesion of 110 MPa and particle friction coefficient of 0.5). The uniaxial compressive strength of this model is 150 MPa, which is close to the upper bound strength of calcite grains, ranging between 120 MPa and 150 MPa [50]. Note that no attempt was made during the calibration process to match the grain strength of the GBM to that of calcite grain. The consistency found between the strength of calcite grains and the strength of the parallel bonded model confirms the applicability of the adopted methodology for calibration of a PFC model with several micro-properties (e.g., GBM).

As mentioned previously and discussed by Bahrani et al. [35], the adopted calibration procedure is an iterative procedure whereby, at each step, the number of trials to achieve an acceptable macro-property was kept to a manageable number by choosing one key micro-property (e.g., smooth-joint tensile strength to match model tensile strength). However, due to the large number of micro-properties included in the GBM and despite the number of imposed constraints explained above, the system is still indeterminate. This means that multiple combinations of micro-properties can lead to equivalently well-calibrated but not unique model. The solution presented here represents such a model that is qualitatively equivalent to other possible solutions. This lack of uniqueness, however, is not seen as a deficiency as combinations of materials with different properties in nature (e.g., different mineralogical assemblage) can also lead to similar behaviors in terms of failure mechanisms, strength and deformability. The model presented here is thus considered a valid model for investigating different aspects of confinement-dependent rock

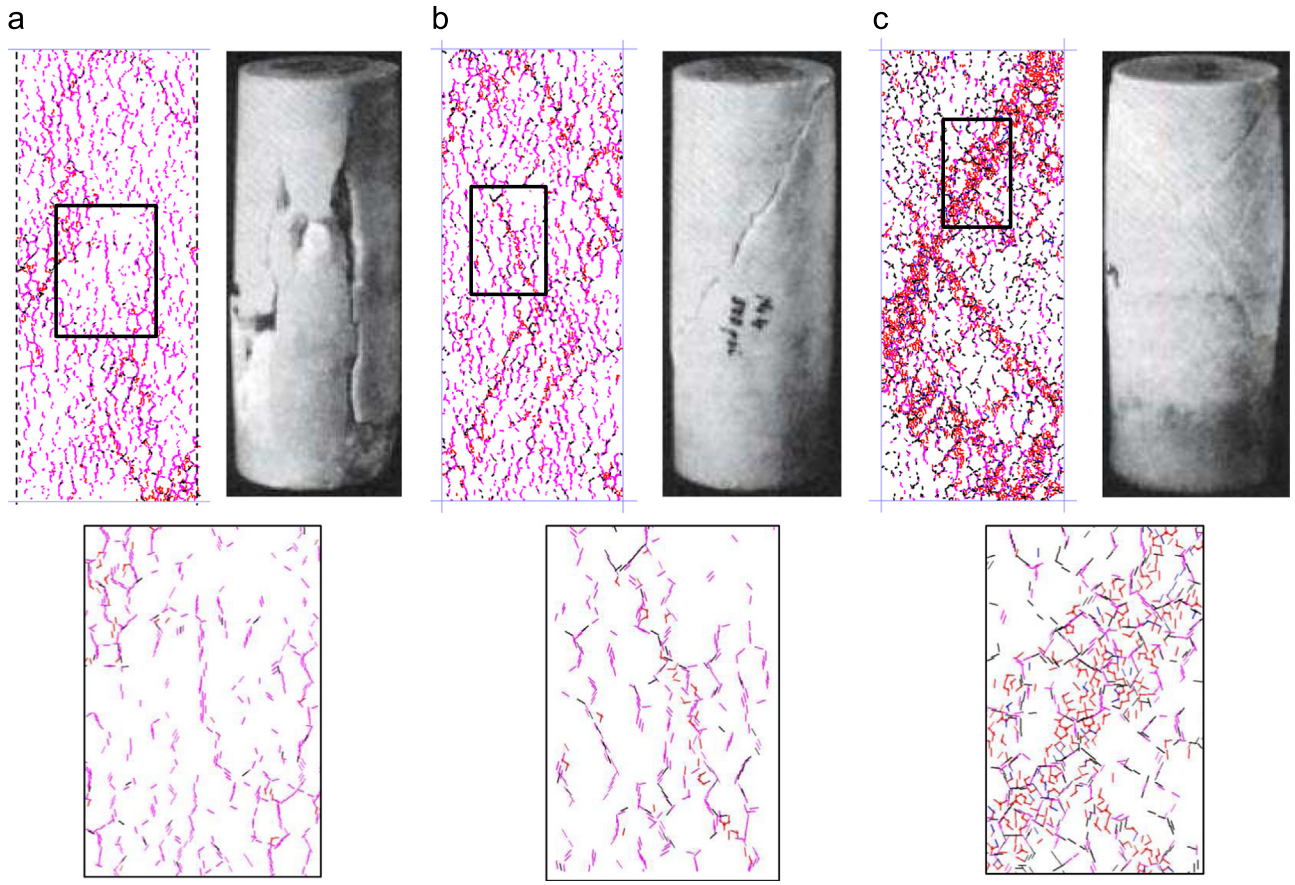

Fig. 11. Comparison between failure modes of intact Wombeyan marble tested by Paterson [6] and those predicted by the grain-based model in (a) unconfined compression, (b) 3.5 MPa confined, and (c) 34.5 MPa confined tests; pink and black refer to inter-grain tensile and shear cracks, respectively, and red and blue refer to intra-grain tensile and shear cracks. The dashed lines in (a) show the sample boundaries. (For interpretation of the references to color in this figure legend, the reader is referred to the web version of this article.)

and rockmass failure processes as long as they remain within the scope, for which the model was calibrated.

5. Failure mode and micro-cracking

The location, orientation, and type of both inter- and intra-grain cracking (tensile and shear) in the models of intact and granulated marble simulated in uniaxial and triaxial compression with 3.5 MPa and 34.5 MPa confining pressures are illustrated in Fig. 11. This figure shows all of the cracks that formed from the beginning of the test to the point when a 20% and 10% stress drop after the peak strength occurred in the post-peak response of unconfined and confined compression tests, respectively.

Grain-based model of intact marble: in the uniaxial compression test (Fig. 11(a)), the cracks are oriented approximately parallel to the axial load direction. Most of the fractures are inter-grain tension cracks. When the crack density was sufficiently high, the interaction of the sub-vertical cracks resulted in a macroscopic nearly axial fracture. In the confined compression tests (Fig. 11(b) and (c)), the interaction between inter- and intra-grain cracks formed macroscopic shear bands. This is more pronounced at higher confinement (Fig. 11(c)), where two major shear fractures developed in the case with 34.5 MPa confining pressure show several intra-grain tensile cracks. The failure modes predicted by the GBM at 0 MPa, 3.5 MPa and 34.5 MPa confining pressures are similar to those observed by Paterson [6] in the laboratory as shown in Fig. 11.

Grain-based model of granulated marble: the assumption in modeling granulated marble was that all the grain boundaries failed during heating process and were in a purely frictional state during the tests. Therefore, only cracks inside grains can be seen during these simulation tests. In the uniaxial compression test (Fig. 12(a)), the model fails mainly by sliding along the grain boundaries, generating large amounts of geometric dilation as can be seen in Fig. 13. Relatively few intra-grain tension cracks are developed at zero confinement. However, a small amount of confining pressure (i.e., 3.5 MPa in Fig. 12(b)) prevents the grains from opening and freely sliding along their boundaries. As a result, the number of intra-grain tension cracks rapidly increases with increasing confinement. This is more pronounced at a confining pressure of 34.5 MPa (Fig. 12(c)), where the interaction between several intra-grain tensile cracks and a number of intra-grain shear cracks generates macroscopic shear fractures similar to those seen in the model of intact marble (compare Fig. 11(c) and Fig. 12(c)).

The stress–strain curves as well as the number of micro-cracks generated for the models of intact and granulated marble deformed in uniaxial and triaxial compression with 3.5 and 34.5 MPa confining pressures are presented in Fig. 14. The following observations can be made from this figure:

(1) The transition from brittle, at zero or low confinement, to more ductile, at high confinement, can be seen in the stress–strain curves, especially in the case of the model of intact marble; (2) failure starts by tensile cracking; inter-grain tensile cracking in the model of intact marble and intra-grain tensile cracking in the model of granulated marble (due to assumed frictional nature of grain contacts, no grain boundary cracks are detectable for the model of granulated marble); (3) the number of shear cracks (inter-grain or intra-grain cracks) increases with increasing confinement; (4) inter- or intra-grain tensile cracks always initiate before inter- or intra-grain shear cracks; and (5) in the model of intact marble, intra-grain tensile cracks initiate before the peak strength is reached, and intra-grain shear cracks initiate in the post-peak region. In the model of granulated marble, the intra-grain shear cracks initiate before peak stress but only at high confinement (i.e., 34.5 MPa).

6. Discussion

6.1. *Influence of interlock on rapid increase in strength at low confinement*

Rosengren and Jaeger [11] noted that the difference between the mechanical behavior of granulated marble and sand arises from the interlocking of grains forming these materials. The interlocking is defined as the constraints limiting the kinematic freedom of the grains, i.e. reducing the ability of particles to rotate and slide along each other. Two types of interlocking are interpreted to generate rapid increase in strength with increasing confinement in the granulated marble: grain surface interlock and grain assembly geometric interlock (called geometric interlock and consequently, related dilation is called geometric dilation).

Grain surface interlock: the non-planarity of the grain boundaries contributes to grain surface interlock. Microscopic examination of the granulated marble by Rosengren and Jaeger [11] showed that this material is composed of tight, highly interlocked calcite crystals with rough surfaces. By analogy with Patton's [46] bilinear shear strength envelope for rough joints, a high dilation

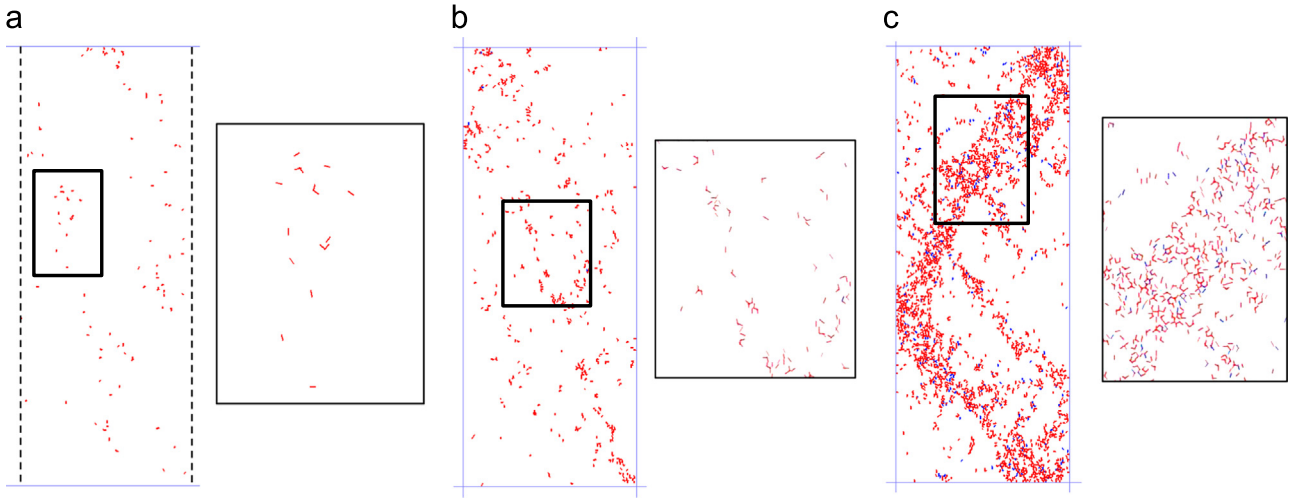

Fig. 12. Failure modes of the grain-based model of granulated marble in (a) unconfined compression, (b) 3.5 MPa confined, and (c) 34.5 MPa confined tests; red and blue refer to intra-grain tensile and shear cracks. The dashed lines in (a) show the sample boundaries. (For interpretation of the references to color in this figure legend, the reader is referred to the web version of this article.)

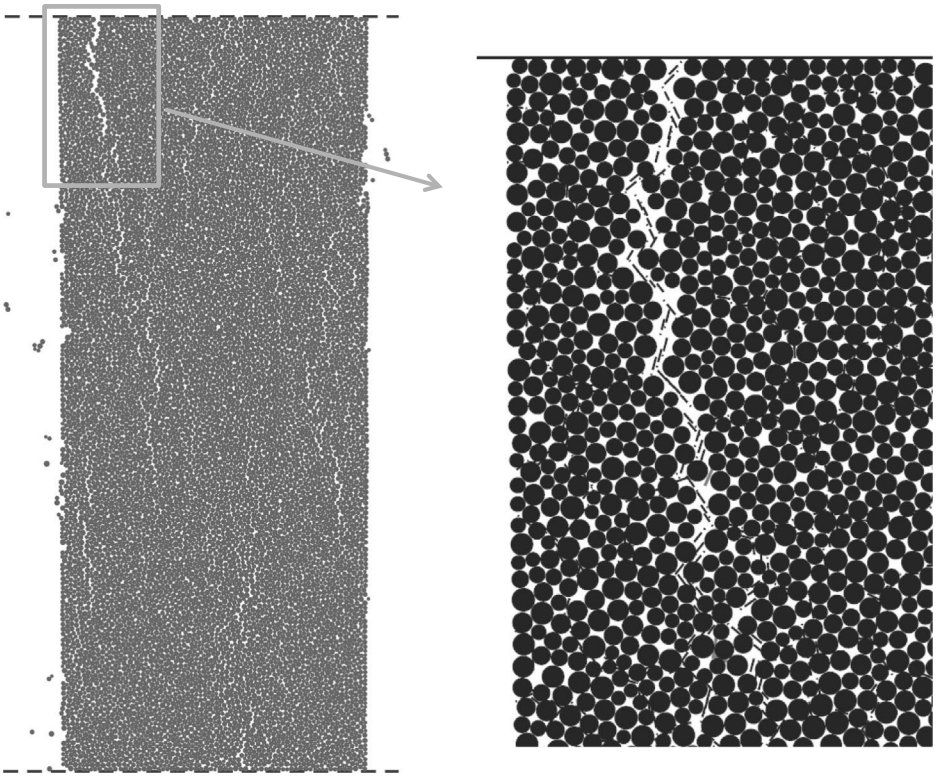

Fig. 13. Macroscopic fractures and large geometric dilation due to opening of grain boundaries in the model of granulated marble in the UCS test (smooth-joint contacts are shown with black lines on the right figure).

due to roughness rapidly increases the shear strength of the grain boundaries as confinement increases. Beyond a critical confinement, dilation due to shear deformation along the boundaries is suppressed and failure occurs by shearing-off asperities and breaking through grains. The surface roughness decreases the ability of grains to slide and rotate during the failure process by increasing the area of contact between grains and limiting kinematic freedom at the grain surface scale. Fig. 15 shows how interlocking level increases with grain irregularity and surface roughness from Fig. 15(a)–(d). Fig. 15(a) shows hexagonal close-packed circular particles with a porosity of 26% (similar to a PFC model with circular particles). In this case, failure occurs by particle rotation and overriding. Fig. 15(b) shows the densely packed rounded sand with a porosity of around 31–34%. The failure in this material occurs by particle rotation, overriding, and minor shearing of asperities. In Fig. 15(c), the interpenetrative contacts in locked sand with a porosity of 27–33% are shown with arrows. The failure of locked sand occurs mainly by particle overriding at low confinement, and by asperity shearing and grain breakage at high confinement. Granulated Wombeyan marble has a porosity of 4% (Fig. 15(d)). Its failure occurs mainly by grain overriding at low confinement, and asperity shearing and grain breakage at high confinement.

Grain geometric interlock: the geometric shape of the grains contributes to the grain geometric interlock. Due to the geometric incompatibilities between the grains, particles cannot easily rotate or slide along each other. This leads to geometric dilation or bulking process that must precede failure. Hence, an extremely high (geometric) dilation leads to a steep failure envelope (as per Patton [46]) at low confinement.

Dusseault and Morgenstern [47,48] noted that the differences between the mechanical behavior of locked sand and dense sand arise from the fabric of granular assemblies. Similar to the granulated marble, the initial portion of the failure envelope of the locked sand has little to no cohesion intercept and the initial slope is extremely steep. Optical and scanning electron microscope investigations by them revealed a dense interpenetrative (concavo-convex) structure and considerable degree of grain surface rugosity (Fig. 15(c)). Athabasca oil sands, St. Peter Sandstone in Minneapolis, and Swan River Sandstone from Manitoba were identified as locked sands [47]. Evidence of good engineering behavior of locked sand in Athabasca Oil Sands including 60 m high and 55° natural slopes, open pit high-walls excavated to depths of 50 m at inclination angles of over 65°, and short term stability of tunnels with no structural support elements was found to be due to the influence of grain assembly geometric interlock and associated large dilation, which result in rapid strength increase with a small amount of confinement.

6.2. Potential practical implications

If the hypothesis advanced in this paper (i.e., that the granulated marble behaves analogous to a non-persistently jointed rockmass with a high block strength) is valid, it follows that the rockmass strength is strongly underestimated by the inappropriate use of GSI-system (Eqs. (1)–(4)) that were developed for isotropic, and persistently jointed rockmasses. The analyses presented in this article suggest that the confined rockmass strength may be at least double, when highly interlocked and confined. The specific implications for pillar strength estimation are briefly discussed next.

The analysis performed by Bahrani and Kaiser [10] and described earlier is summarized in Fig. 16. As can be seen in this figure, when GSI of 73 is used to match the strength reduction of granulated marble from that of intact marble at zero confinement, the confined strength of the granulated marble is underestimated by a factor of 2–4 depending on confinement. Bahrani and Kaiser [10] suggested the use of $m_b=11$ instead of 2.05 obtained by Eq. (3), and $a=0.34$ instead of 0.5 obtained by Eq. (4) to fit to the strength of granulated marble for the entire range of confinement.

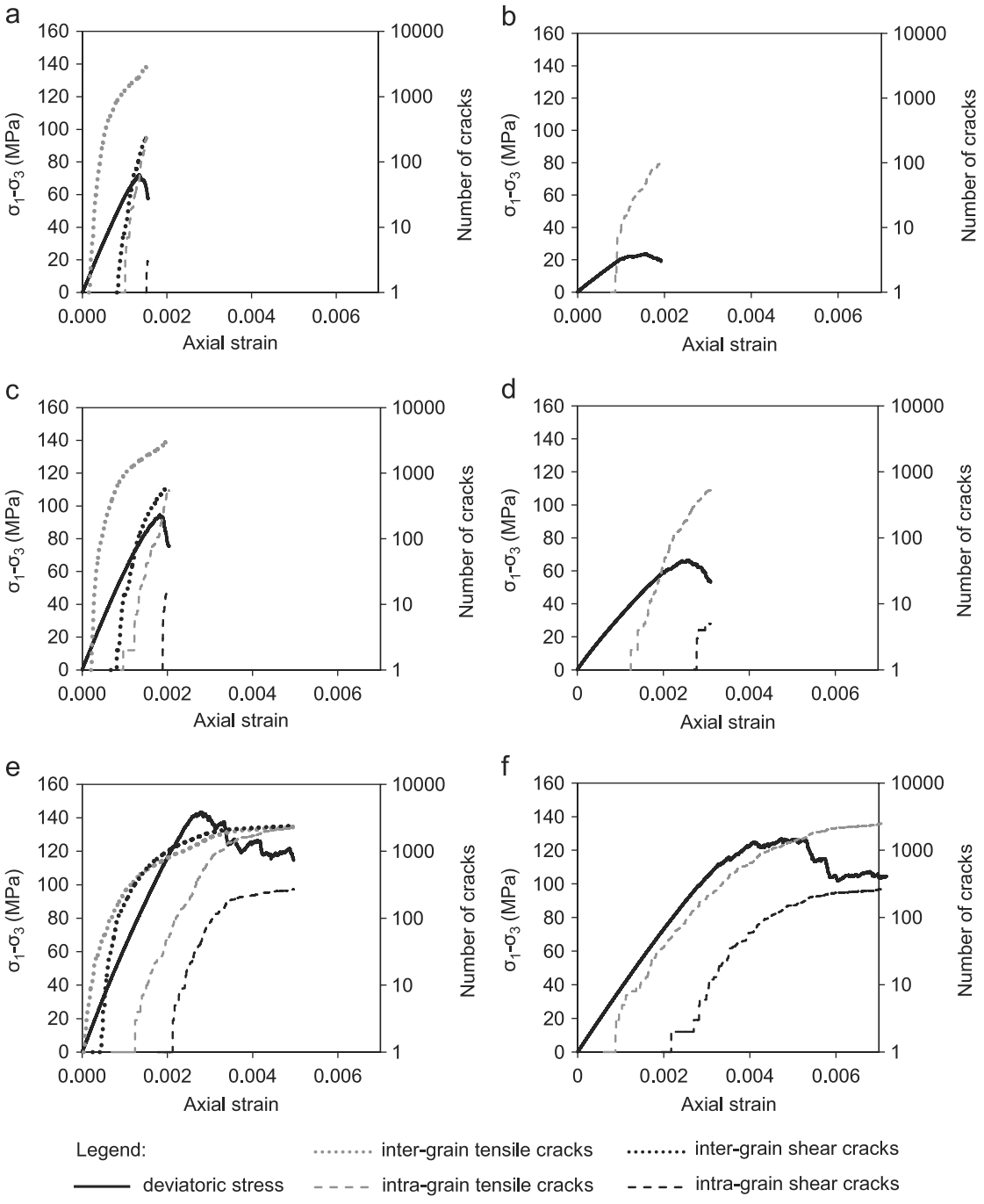

Fig. 14. Stress–strain curves and numbers of inter- and intra-grain tensile and shear cracks for: (a) intact GBM at zero confining pressure, (b) granulated GBM at zero confining pressure, (c) intact GBM at 3.5 MPa confining pressure, (d) granulated GBM at 3.5 MPa confining pressure, (e) intact GBM at 34.5 MPa confining pressure, and (f) granulated GBM at 34.5 MPa confining pressure.

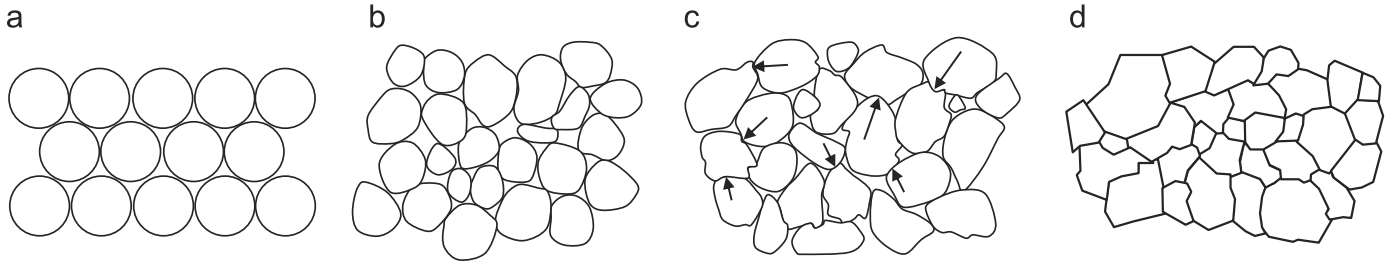

Fig. 15. Fabric of granular assemblies with increasing interlock from left to right: (a) hexagonal close-packed circular particles, (b) densely packed rounded sand, (c) locked sand with interpenetrative contacts shown with arrows, and (d) granulated Wombeyan marble. a–c redrawn and modified from [47], and d drawn from [11].

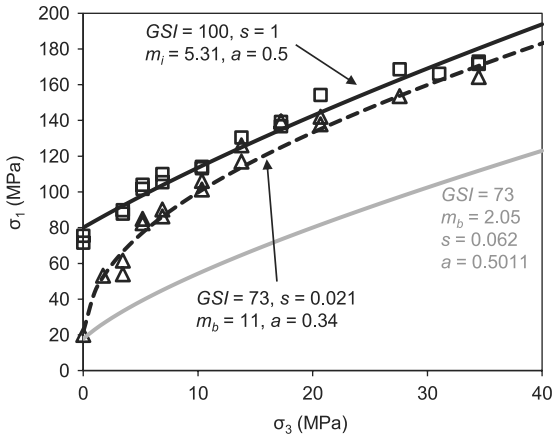

Fig. 16. Fitted data from tests on intact and granulated Wombeyan marble [12] with adjusted Hoek–Brown rockmass parameters; squares for intact and triangles for granulated.

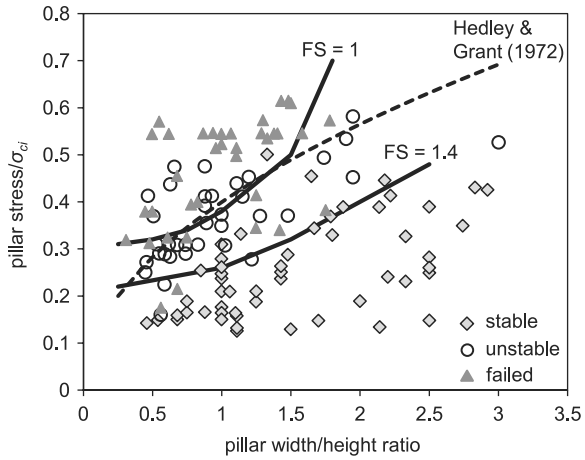

Fig. 17. Pillar stability graph showing stable, unstable and failed pillars together with one of many empirical stability criteria [55] and stability limits obtained by continuum modeling using Hoek–Brown brittle parameters (modified from [56]).

In this figure the strength difference between the Hoek–Brown strength envelope (i.e., gray line) and the envelope for the rockmass analogue (i.e., dashed line through granulated marble data) becomes most relevant for the design of wide pillars with confined pillar core and confined abutments at depth. As discussed by Valley et al. [51] and Kaiser et al. [52], using a strength envelope that properly captures the strength increase with confinement will lead to an optimized design of pillars. On the other hand, if the strength of a pillar core is underestimated (i.e., by applying the GSI-system designed for persistently jointed rockmass), such pillars may not yield and accumulate stress, thus becoming burst prone.

Evidence of a significant increase in rockmass strength at higher confinement can be found in the pillar stability graph developed by Lunder and Pakalnis [53], based on the data collected by Potvin et al. [54], which is extensively used by the mine engineers for the design of mine pillars. This graph, shown in Fig. 17, summarizes failed, transitional (unstable), and stable pillars, and suggests that no failed pillar can be identified at pillar width to height ratios greater than 1.8. This is interpreted here as an indication of elevated rockmass strength in the wide pillar cores due to confinement.

Hedley and Grant [55] suggested a criterion that flattens with increasing pillar width to height ratio for pillar strength normalized by the unconfined strength of the intact rock (shown with dashed line in Fig. 17). Intuitively, by considering the rise in rockmass strength with confinement, it would be expected that wide pillars with high confinement in core should have strengths that exceeds the unconfined intact rock strength if non-persistently jointed and highly interlocked, suggesting a criterion that steepens with increasing width to height ratio.

Such an increase in pillar strength with increasing confinement (pillar width) was suggested by Martin and Maybee [56] (solid black lines for factors of safety of 1 and 1.4). They used the brittle Hoek–Brown parameters ($m_b=0$, $s=0.11$) suggested by Martin et al. [57] and elastic models to arrive at the conclusion that the data should be fitted by convex functions. Their approach is basically assessing the potential for pillar wall failure and considers the depth of failure as a measure of pillar wall degradation and results in a good agreement with the field data. Indirectly, their work also implies that the pillar cores for width to height ratios exceeding about two are sufficiently stable to prevent further propagation of wall spalling. If this was not the case and pillar cores were yielding, failed pillars should be found at width to height ratios greater than 2. Because of the use of elastic models, their approach does not capture the failure process in the core and cannot be applied to rockmasses with different levels of block interlocking or discontinuity surface conditions (i.e., different GSI-values).

For pillar design in non-persistently jointed rockmasses with a high degree of interlock, it is therefore necessary to develop the means to obtain the failure envelope that better captures the rapid strengthening effect due to confinement. The GBM presented here seems to be suitable to assess the strength of pillar cores. Further research is currently being pursued on the use of calibrated GBM to simulate rockmasses with different levels of damage and the results will then be used to develop means to estimate the parameters for strength estimation of highly interlocked, non-persistently jointed rockmasses.

7. Conclusions

The PFC2D grain-based model was used to simulate the laboratory response and mechanical properties of intact and granulated Wombeyan marble. The term 'granulated' refers to a heat treated sample where the grain boundaries were separated. Due to the random locations of the grain boundaries, grain geometry, and the roughness of grain boundaries, the granulated marble is considered to be an analogue for a highly interlocked, non-persistently jointed rockmass. After calibrating the intact and granulated GBMs to the laboratory properties of intact and granulated Wombeyan marble, the following was concluded:

(1) The PFC2D–GBM captures the laboratory observed transition in the failure mode of brittle rocks from axial fracturing at low confinement to shear fracture formation at high confinement; (2) the PFC2D–GBM captures the laboratory observed stress–strain response of brittle rocks from brittle behavior (stress drop after peak) at low confinement to ductile behavior (maintenance of peak strength post-peak) with increasing confinement; and (3) rock failure processes include fracturing which mainly initiates along the grain boundaries and continues by breaking through the grains as the axial stress reaches and passes the peak stress. The failure process is dominated by tensile cracking. The number of cracks generated by shear stress (i.e., shear cracks) increases with increasing confinement.

The rapid increase in strength with confinement observed in the granulated Wombeyan marble and similar materials (e.g., locked sands) is due to interlocking and the resultant high geometric dilation, which can be suppressed in strong rocks beyond a critical confining pressure. Two interlocking processes are observed in the granulated marble, i.e., grain surface interlock (due to surface roughness) and grain assembly geometric interlock (due to grain or block geometric factors).

The results described in this paper have implications for the estimation of the strength of highly confined non-persistently jointed hard rockmasses. Whereas the GSI-system is well-calibrated and proven to be helpful for the engineering design of support in tunnels and caverns in weak rocks and persistently jointed rockmasses, the findings presented in this paper suggest that the resulting confined rockmass strength may be significantly underestimated for highly interlocked, non-persistently jointed rockmasses. Hence, the strength of wide pillars may be significantly underestimated when strength parameters are adopted based on the conventional GSI-system parameters.

Acknowledgments

This research project is supported by the Rio Tinto Centre for Underground Mine Construction at CEMI, Itasca Consulting Group through its Itasca Education Partnership (IEP) program and the Natural Sciences and Engineering Research Council of Canada (NSERC). Drs. Matthew Pierce and David Potyondy, and Rob Bewick are acknowledged for many insightful discussions and reviewing different versions of manuscript.

References

[1] Hoek E. Strength of rock and rock masses. ISRM News J 1994;2(2):4–16.
[2] Hoek E, Kaiser PK, Bawden WF. Support of underground excavations in hard rock. Rotterdam: Balkema; 1995.
[3] Hoek E, Brown ET. Empirical strength criterion for rock masses. J Geotech Eng ASCE 1980;106:1013–35.
[4] Hoek E, Brown ET. Underground excavations in rock. London: Institution of Mining and Metallurgy; 1980.
[5] Hoek E, Brown ET. Practical estimates of rock mass strength. Int J Rock Mech Min Sci 1997;34(8):1165–86.
[6] Paterson MS. Experimental deformation and faulting in Wombeyan marble. Geol Soc Am Bull 1958;69:465–76.
[7] Elmo D, Stead D. An integrated numerical modeling-discrete fracture network approach applied to the characterisation of rock mass strength of naturally fractured pillars. Rock Mech Rock Eng 2010;43:3–19.
[8] Mas Ivars D, Pierce ME, Darcel C, Reyes-Montes J, Potyondy DO, Young RP, et al. A synthetic rock mass approach for jointed rock mass modeling. Int J Rock Mech Min Sci 2011;48:219–44.
[9] Hoek E, Carranza-Torres C, Corkum B. Hoek–Brown failure criterion – 2002 edition. In: Proceedings of NARMS-TAC conference, Toronto; 2002. p. 267–73.
[10] Bahrani N, Kaiser PK. Strength degradation of non-persistently jointed rock-mass. Int J Rock Mech Min Sci 2013;62:28–33.
[11] Rosengren KJ, Jaeger JC. The mechanical properties of an interlocked low-porosity aggregate. Géotechnique 1968;18:317–26.
[12] Gerogiannopoulos NG. A critical state approach to rock mechanics [Ph.D.thesis]. University of London; 1976 (325 p.).
[13] Gerogiannopoulos NG, Brown ET. The critical state concept applied to rock. Int J Rock Mech Min Sci 1978;15:1–10.
[14] Yang SQ, Jiang YZ, Xu WY, Chen XQ. Experimental investigation on strength and failure behavior of pre-cracked marble under conventional triaxial compression. Int J Solids Struct 2008;45:4796–819.
[15] Martin CD, Stimpson B. The effect of sample disturbance on laboratory properties of Lac du Bonnet granite. Can Geotech J 1994;31:692–702.
[16] Cundall PA. A computer model for simulating progressive, large scale movements in blocky rock systems. In: Proceedings of the symposium international society for rock mechanics, No. 2:8, Nancy; 1971.
[17] Cundall PA, Strack ODL. A discrete numerical model for granular assemblies. Géotechnique 1979;29:47–65.
[18] Itasca Consulting Group Inc., Particle Flow Code in 2 dimensions (PFC2D), Version 4.0. Minneapolis; 2008.
[19] Itasca Consulting Group Inc., Particle Flow Code in 3 dimensions (PFC3D), Version 4.0. Minneapolis; 2008.
[20] Potyondy DO, Cundall PA. A bonded particle model for rock. Int J Rock Mech Min Sci 2004;41:1329–64.
[21] Potyondy DO. The bonded-particle model as a tool for rock mechanics research and application: current trends and future directions. In: Proceedings of the 7th Asian rock mechanics symposium, Seoul, Korea; 2012. p. 73–105.
[22] Diederichs MS. Instability of hard rock masses: the role of tensile damage and relaxation [Ph.D. thesis]. University of Waterloo; 1999 (617 p).
[23] Wang Y, Tonon F. Modeling Lac du Bonnet granite using a discrete element model. Int J Rock Mech Min Sci 2009;46:1124–35.
[24] Bout DF, McPherson BJOL. Simulation of sedimentary rock deformation: lab-scale model calibration and parameterization. Geophys Res Lett 2002;29(4):1054.
[25] Yoon J. Application of experimental design and optimization to PFC model calibration in uniaxial compression simulation. Int J Rock Mech Min Sci 2007;44:871–89.
[26] Wang Y, Tonon F. Calibration of a discrete element model for intact rock up to its peak strength. Int J Numer Anal Methods Geomech 2010;34:447–69.
[27] Cho N, Martin CD, Sego DC. A clumped particle model for rock. Int J Rock Mech Min Sci 2007;44:997–1007.
[28] Yoon JS, Jeon S, Zang A, Stephansson O. Bonded particle model simulation of laboratory rock tests for granite using particle clumping and contact unbonding. Paper: 08-05. In: Continuum and Distinct Element Numerical Modeling in Geomechanics, Minneapolis; 2011.
[29] Yoon JS, Zang A, Stephansson O. Simulating fracture and friction of Aue granite under confined asymmetric compressive test using clumped particle model. Int J Rock Mech Min Sci 2012;49:68–83.
[30] Bahrani N, Valley B, Kaiser PK. Discrete element modeling of drilling-induced core damage and its influence on laboratory properties of Lac du Bonnet granite. In: Proceedings of the 45th US rock mechanics symposium, San Francisco; 2011. 9 p.
[31] Mosher S, Berger RL, Anderson DE. Fracture characteristics of two granites. Rock Mech 1975;7:167–76.
[32] Erarsalan N, Williams DJ. Investigating the effect of cyclic loading on the indirect tensile strength of rocks. Rock Mech Rock Eng 2012;45:327–40.
[33] Gatelier N, Pellet F, Loret B. Mechanical damage of an anisotropic porous rock in cyclic triaxial tests. Int J Rock Mech Min Sci 2002;39:335–54.
[34] Potyondy DO. A grain-based model for rock: approaching the true microstructure. In: Proceedings of the rock mechanics in the Nordic Countries; 2010. 10 p.
[35] Bahrani N, Valley B, Kaiser PK, Pierce M. Evaluation of PFC2D grain-based model for simulation of confinement-dependent rock strength degradation and failure processes. In: Proceedings of the 45th US rock mechanics symposium, San Francisco, CA, USA; 2011. 10 p.
[36] Bahrani N, Potyondy D, Pierce M. Simulation of Brazilian test using PFC2D grain-based model. In: 21st Canadian rock mechanics symposium: RockEng 12 – Rock Engineering for Natural Resources, Edmonton: Canada; 2012.
[37] Bewick RP, Kaiser PK, Bawden WF, Bahrani N. DEM simulation of direct shear: 1. Rupture under constant normal stress boundary conditions. Rock Mech Rock Eng 2013. http://dx.doi.org/10.1007/s00603-013-0490-8.
[38] Bewick RP, Kaiser PK, Bawden WF. DEM simulation of direct shear: 2. Grain boundary and mineral grain strength component influence on shear rupture. Rock Mech Rock Eng 2013. http://dx.doi.org/10.1007/s00603-013-0494-4.
[39] Hadjigeorgiou J, Esmaieli K, Grenon M. Stability analysis of vertical excavations in hard rock by integrating a fracture system into a PFC model. Tunn Undergr Space Technol 2009;24:296–308.
[40] Esmaieli K, Hadjigeorgiou J, Grenon M. Estimating geometrical and mechanical REV based on synthetic rock mass models at Brunswick Mine. Int J Rock Mech Min Sci 2010;47:915–26.
[41] Chiu C, Wang T, Weng M, Huang T. Modeling the anisotropic behavior of jointed rock mass using a modified smooth-joint model. Int J Rock Mech Min Sci 2013;62:14–22.
[42] Bahrani N, Purvance M, Emam S. A comparison between 2D and 3D bonded-particle models for rock. In: Proceedings of the 47th US rock mechanics symposium, San Francisco; 2013. 10 p.
[43] Bieniawski ZT, Bernede MJ. Suggested methods for determining the uniaxial compressive strength and deformability of rock materials. Int J Rock Mech Min Sci 1979;16:138–40.
[44] Martin CD, Chandler NA. The progressive fracture of Lac du Bonnet granite. Int J Rock Mech Min Sci 1994;31:643–59.
[45] Hajiabdolmajid V, Kaiser PK, Martin CD. Modelling brittle failure of rock. Int J Rock Mech Min Sci 2002;39:731–41.
[46] Patton FD. Multiple mode of shear failure in rock. In: Proceedings of the 1st international conference on rock mechanics, Lisbon; 1966. p. 509–11.
[47] Dusseault MB, Morgenstern NR. Shear strength of Athabasca oil sands. Can Geotech J 1978;15:16–38.
[48] Dusseault MB, Morgenstern NR. Locked sands. Q J Eng Geol Hydrogeol 1979;12:117–31.
[49] Wei Y, Anand L. On micro-cracking, inelastic dilatancy, and the brittle ductile transition in compact rocks: a micro-mechanical study. Int J Solids Struct 2008;45:2785–98.
[50] Lama RD, Vutukuri VS. Handbook on mechanical properties of rocks. Clausthal: Trans. Tech. Publications; 1978.
[51] Valley B, Kim B, Suorineni FT, Bahrani N, Bewick R, Kaiser PK. Influence of confinement dependent failure processes on rock mass strength at depth. In: Proceedings of the ISRM 12th International Congress on Rock Mechanics, Beijing, China; 2011. 6 p.
[52] Kaiser PK, Kim B, Bewick RP, Valley B. Rock mass strength at depth and implications for pillar design. Trans Inst Min Metall A 2011;120(3):170–9.
[53] Lunder PJ, Pakalnis R. Determination of the strength of hardrock mine pillars. Bull Can Inst Min Metall 1997;90:51–5.
[54] Potvin Y, Hudyma MR, Miller HDS. Design guidelines for open stope support. Bull Can Inst Min Metall 1989;82:53–62.
[55] Hedley DGF, Grant F. Stope-and-pillar design for the Elliot Lake Uranium Mines. Bull Can Inst Min Metall 1972;65:37–44.
[56] Martin CD, Maybee WG. The strength of hard rock pillars. Int J Rock Mech Min Sci 2000;37:1239–46.
[57] Martin CD, Kaiser PK, McCreath DR. Hoek–Brown parameters for predicting the depth of brittle failure around tunnels. Can Geotech J 1999;36:136–51.